

Volumetric and Size Characterization of Void Morphologies in Thermally Sprayed Metallic Deposits Using Scattering Techniques

T. Keller, W. Wagner, Villigen-PSI /CH, J. Ilavsky, College Park /USA, A.J. Allen, Gaithersburg /USA
N. Margadant, S. Siegmann Thun /CH, Barbezat, Wohlen /CH, J. Pisacka, Prague /CR, R. Enzl, Plzen /CR

The complex void microstructures of thermally sprayed deposits may be approximated by three major void systems (interlamellar pores, intralamellar cracks, and volumetric globular voids), each with different volume fractions, anisotropies, sizes and shapes. This complex void morphology is expected to have a strong influence on the properties of thermally sprayed coatings. NiCrAlY deposits manufactured by vacuum-, atmospheric- and water-stabilized plasma spraying and flame spraying techniques have previously been investigated by small angle neutron scattering (SANS) in the Porod scattering regime. A relationship between the void specific surface area obtained and wear resistance was revealed. To characterize the void system in more detail, the technique of multiple small angle neutron scattering (MSANS), previously applied to thermally sprayed ceramic coatings, was applied to the metallic NiCrAlY deposits. The above-mentioned three-component void morphology was assumed based on empirical considerations and on analysis of SEM micrographs of coating cross-sections. The model results suggest the interlamellar pores to be most significant in the overall void system. For the atmospheric-plasma sprayed metallic deposit, only a small void volume fraction is found in the fine intralamellar crack system. For the water-stabilized-plasma sprayed deposit, intralamellar cracks are found to be essentially absent, and both anisotropic systems are interpreted to be comprised of interlamellar pores.

1 Introduction

The microstructure of thermally sprayed deposits, and therefore their material properties, are to a large extent related to the internal void structure. Important parameters are the total void volume fraction and the total specific surface area of the voids. Of further interest are usually average pore sizes as well as orientations of anisotropically shaped pores. Small-angle neutron scattering (SANS) techniques can provide information on the total specific surface area and, in principal, also direct size information on voids of up to a about 100 nm. The complex void structure of many thermal spray deposits extends over a size regime up to a few micrometers in diameter, that does not allow a direct determination of pore size by this method. Nevertheless, the total specific surface area can still be obtained in the Porod regime [1].

A method has been developed to deduce average pore sizes and orientational distributions by the technique of multiple small-angle neutron scattering (MSANS). The analysis employs the experimentally determined wavelength-dependent broadening of the primary neutron beam when it passes through the sample and the neutrons undergo copious multiple scattering. Recently this method was extended to model the void structure of thermally sprayed deposits, allowing for the three distinct void subsystems often predominant in such coatings. This method then was successfully applied to ceramic deposits [2]. In the present investigation, the MSANS technique was applied to an atmospheric plasma- and a water-stabilized plasma-spray *metallic* NiCrAlY deposit. The total specific surface area was determined previously from SANS measurements [3]. Here, the MSANS technique is described and references for the theoretical background are given. The results from modelling the void microstructures of the two investigated deposits are presented and compared.

2 Experimental

2.1 Samples

The results presented here are obtained from investigations of an atmospheric plasma- (APS) and a water-

stabilized plasma- (WSP) sprayed metallic NiCrAlY deposit. The chemical composition of the feedstock material was 67% Ni, 22% Cr, 10% Al, 1% Y, where all values are given in mass fractions. Both deposits were sprayed using optimized spray parameters with the spray direction perpendicular to the surface of mild steel substrates. By cutting and grinding, 2.30 mm and 2.27 mm thick slices for the APS deposit and WSP deposit, respectively, were prepared as cross-section samples. From the remaining sample the deposits were removed from the substrate by wire-electro discharge machining to obtain free-standing deposits. The total porosity of the deposits was determined by precision density measurements [4]. The cross-section samples were investigated with the neutron beam passing through the deposit perpendicular to the spray direction. The free standing deposits were measured with the neutron beam parallel to the spray direction using stacks of samples to obtain sufficient thicknesses along the beam path, 2.06 mm and 3.76 mm for the APS and WSP deposits, respectively. The oxide content of the APS and WSP NiCrAlY deposits were measured by the hot extraction method to be below 1 wt% [4], indicating a negligible contribution from neutron scattering on oxides as a third phase. The neutron scattering experiments were performed at the 8 m SANS instrument [5] at the Centre for Neutron Research, National Institute of Standards and Technology, Gaithersburg, MD, USA.

2.1 Total specific surface area from SANS

As previously described [3], the total specific surface areas were obtained by SANS in the Porod regime [6] according to

$$\langle d\Sigma/d\Omega(\mathbf{Q}) \rangle = 2\pi |\Delta\rho|^2 S_{\text{tot}}/Q^4$$

where $d\Sigma/d\Omega(\mathbf{Q})$ is the calibrated absolute intensity or macroscopic scattering cross-section, \mathbf{Q} the scattering vector, and $|\Delta\rho|^2$ the scattering contrast between the metal matrix and the voids. $\langle \rangle$ stands for an orientational average of the sectors over all azimuthal angles, exploiting the axial symmetry of the microstructure about the spray direction. S_{tot} is the total specific surface area. The magnitude of \mathbf{Q} is given by $|\mathbf{Q}| = Q = 4\pi \sin \theta/\lambda$, where θ is half the scattering

angle and λ is the wavelength of the neutrons. To determine the total specific surface area in the Porod regime, a wavelength of $\lambda = 8 \text{ \AA}$ was used. For all measurements the wavelength resolution was $\Delta\lambda/\lambda = 0.15$. The scattering contrast of the NiCrAlY alloy with the voids, $|\Delta\rho|^2 = 41.34 \times 10^{28} \text{ m}^{-4}$, was determined from the chemical composition of the feedstock powder and a skeletal density of $(7.25 \pm 0.07) \text{ g cm}^{-3}$, determined by helium pycnometry [4].

2.1 Size and orientation information from MSANS

When neutrons pass through a void within a homogeneous matrix, diffraction and refraction effects occur. The resulting deflection depends on the wavelength of the incoming neutrons, the size and shape of the void, and its scattering contrast with the matrix. If the deposit is thick enough and the void volume fraction within the matrix is sufficiently high, the neutrons are scattered many times.

This results in a broadening of the primary neutron beam when it passes through the sample. The multiple small-angle neutron scattering beam-broadening [2,7,8,9] can be expressed in terms of the radius of curvature, r_c , of the scattering curve at $Q=0$:

$$r_c = \lim_{Q \rightarrow 0} \left[\frac{W''(\mathbf{Q}, \tau)}{W(\mathbf{Q}, \tau)} \right]^{-1/2}$$

Here, $W(\mathbf{Q}, \tau)$ is the profile of the neutron beam as a function of the scattering vector \mathbf{Q} and sample thickness τ after passing through the sample, and $W''(\mathbf{Q}, \tau)$ represents a double derivative with respect to \mathbf{Q} . The wavelength-dependence is implicitly given by the dependence of r_c on the magnitude of \mathbf{Q} . r_c can be shown to be numerically equivalent to the standard deviation of a Gaussian fit to the beam profile at low Q . In the following, r_c is referred to as the (MSANS) beam-broadening of a deposit for a given wavelength and orientation with respect to the neutron beam. To account experimentally for the instrumental resolution width r_{pb} of the primary beam, r_c has to be corrected from the measured width r_{sample} by

$$r_c = \sqrt{r_{\text{sample}}^2 - r_{pb}^2}$$

For anisotropic microstructures, the broadening depends also on the direction of \mathbf{Q} . The MSANS anisotropy can be expressed in terms of the aspect ratio of an ellipse, fitted to the anisotropic r_c data.

The MSANS beam-broadening at wavelengths of 12 \AA , 13 \AA , 14 \AA , 15 \AA , 16 \AA , 17 \AA and 18 \AA was determined for both, the cross-section samples and the free-standing deposits. Due to the axial symmetry of the microstructure in the spray direction, the MSANS beam-broadening of the free-standing sample is found to be circularly-symmetric and is therefore radially averaged about the incident beam. The anisotropic

MSANS broadening of the cross-section sample was radially averaged about the incident beam as well, resulting in a circular-average of the orientation distributions of the spheroidal shaped pores in the cross section plane. In addition, to analyze the MSANS anisotropy, the MSANS data for the cross-section samples were sector-averaged in 15° wide sectors, and an ellipse was fitted to the data.

The void structure was modelled to fit the orientationally-averaged MSANS beam-broadening r_c data obtained for the two sample orientations, consistent with the total porosity. Further constraints for the model were the (Porod) total specific surface area experimentally-determined from SANS and the observed MSANS anisotropy.

3 Results

To model the MSANS broadening under the constraints discussed above, the total void volume fraction is split into three distinct void subsystems, two of them consisting of oblate spheroidal elements, and the third one being globular pores. The spheroidal elements are described by a radius R and an aspect ratio β . The maximum opening dimension is thus $2\beta R$, and the mean opening dimension is $\langle O.D. \rangle = 4\beta R/3$.

The important size information that the MSANS method allows to be deduced is the mean opening dimension. The short dimension of each spheroid produces the most significant part of the broadening and this fact permits the simplified assumption that the two spheroidal void systems can be described by β values of 1/10 and 1/5. While for the globular pores the mean radius R_G can be regarded as the real size of the pore, for the spheroids it is rather the mean opening dimension

$$\langle O.D. \rangle = 4\beta \langle R \rangle / 3$$

that is meaningful in terms of microstructure. To account for the orientation distributions of the two spheroidal element systems, possible orientations are subdivided, in each case, into angular ranges with respect to the spray direction: 0°-30°, 30°-60° and 60°-90°. The probabilities of finding a crack or pore within each of these ranges are given by g_L , g_M , and g_H , respectively. Due to the possible orientation of each spheroidal element within the full solid angle, for a random distribution, $g_L = 0.134$, $g_M = 0.366$ and $g_H = 0.5$. The mean sizes of the elements used to model the three void systems were parameterized by the ratios of their large dimensions with respect to each other. For the APS and WSP deposits modelled here, suitable ratios were found to be: $\langle R \rangle_p / \langle R \rangle_c = 1.0$ and $\langle R \rangle_g / \langle R \rangle_c = 1.3$, where the index c stands for the system of flat voids with $\beta = 1/10$, p for the interlamellar void system with $\beta = 1/5$ and g for the globular pores.

3.1 Atmospheric plasma sprayed deposit

By SANS analysis in the Porod regime the total specific surface area was determined to be $S_{\text{tot}} = (0.766 \pm 0.010) \times 10^6 \text{ m}^2 \text{ m}^{-3}$. The total volume fraction was found to be 0.081 ± 0.001 . The experimentally determined circularly-averaged MSANS beam-broadening is shown in Fig. 1 for the cross-section and free-standing deposit. Model and experimental anisotropies are displayed in the polar plot of Fig. 2. The MSANS anisotropy of the cross-section sample, determined by averaging the aspect ratios of the ellipses for all wavelengths was found experimentally to be 1.35 ± 0.03 .

By non-linear least-squares fitting, the average large radius of the $\beta=1/10$ void system, being the only remaining free fitting parameter, was found to be $R_C = (0.728 \pm 0.010) \mu\text{m}$ [10], keeping all other constraints fulfilled: the model MSANS anisotropy is 1.38, and the total specific surface area for the model is found to be $0.769 \times 10^6 \text{ m}^2 \text{ m}^{-3}$. The mean opening dimensions of the spheroidal pore systems together with their mean orientation distributions and the mean globular pore radius obtained by the model fit are given in Table 1.

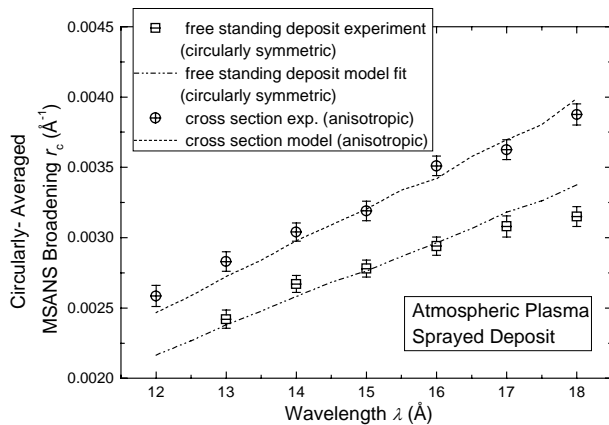


Fig. 1. Beam broadening of the APS deposit. Model results and experimental data are displayed for the neutron beam parallel and perpendicular to the spray direction.

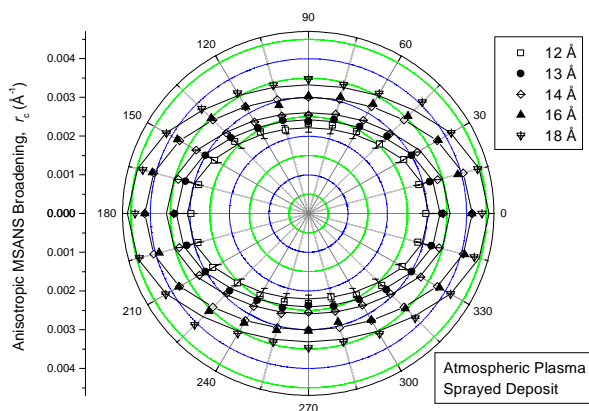


Fig. 2. Anisotropic MSANS beam-broadening for the APS cross-section sample as measured and predicted by the model for different wavelengths. Standard deviations of the experimental data are indicated for $\lambda = 12 \text{ \AA}$.

The fraction of specific surface area and void volume within the different void subsystems are compared in Table 2. Estimated fractional standard deviations are $\pm 10\%$ for the component porosities, and $\pm 5\%$ for the probabilities of finding a pore orientation within one of the three ranges, the component surface areas, the $\langle \text{O.D.} \rangle$ values, and the mean globular pore diameter. The model results are qualitatively confirmed by the SEM micrograph of the APS cross-section displayed in Fig. 3, where globular pores within the metal matrix can be identified as well as interlamellar pores with opening dimensions of the order of the model predictions, and only a few cracks are apparent.

Table 1. Modelled mean opening dimensions and orientation distributions of the void subsystems of the APS deposit.

	$\langle \text{O.D.} \rangle$ (μm)	$\langle 2R_C \rangle$ (μm)	g_L	g_M	g_H
$\beta = 1/10$	0.097	-	0.04	0.22	0.74
$\beta = 1/5$	0.194	-	0.64	0.31	0.05
Globular pores	-	1.892	-	-	-

Table 2. Specific surface areas and volume fractions of the three void subsystems of the APS deposit, calculated from the MSANS model parameters.

	Specific surface area [$10^6 \text{ m}^2 \text{ m}^{-3}$]	Volume fraction
$\beta = 1/10$	$0.127 \cong 17\%$	7 %
$\beta = 1/5$	$0.563 \cong 73\%$	62 %
Globular pores	$0.079 \cong 10\%$	31 %
Σ_{total}	$0.769 \cong 100\%$	$0.081 \cong 100\%$

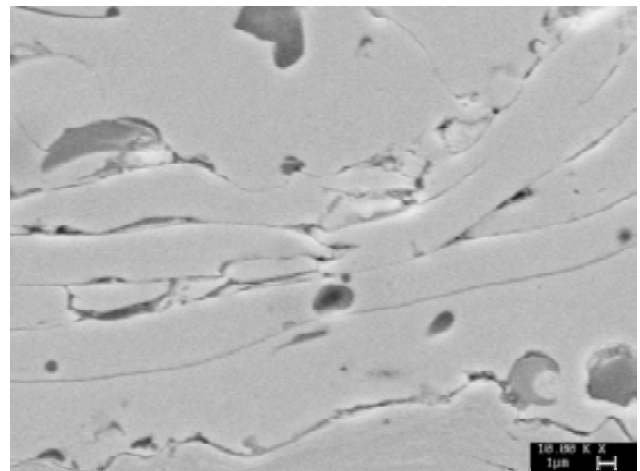


Fig. 3. SEM micrograph of a polished cross-section of the APS NiCrAlY deposit. The spray direction is vertical.

3.2 Water-stabilized plasma sprayed deposit

The experimentally determined total specific surface area was found to be $S_{\text{tot}} = (1.26 \pm 0.01) \times 10^6 \text{ m}^2 \text{ m}^{-3}$. The total volume fraction was determined to be 0.119 ± 0.001 . The circularly-averaged MSANS beam-broadening is shown in Fig. 4 for the cross-section and free-standing deposit. Model and experimental anisotropies are displayed in the polar plot of Fig. 5. The MSANS anisotropy of the cross-section sample, determined by averaging the aspect ratios of the ellipses for all wavelengths was found experimentally to be 1.25 ± 0.03 .

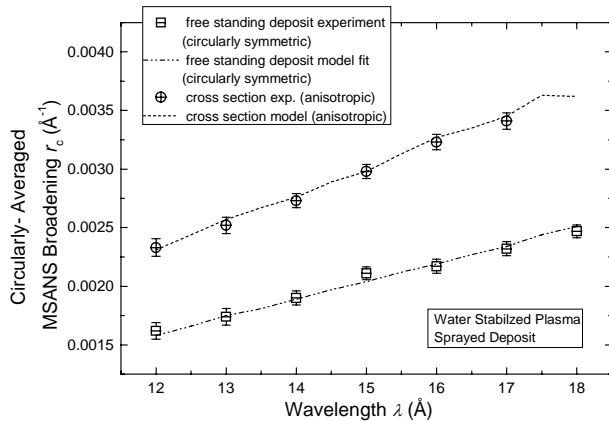


Fig. 4. Beam broadening of the WSP deposit. Model results and experimental data are displayed for the neutron beam parallel and perpendicular to the spray direction.

The microstructural modelling of the WSP deposit allowed a fit satisfying all constraints only for similar orientation distributions of the two spheroidal shaped pore systems. $R_C = (1.008 \pm 0.010) \mu\text{m}$ is found by the fitting for the radius of the $\beta = 1/10$ void system. The model total specific surface area is calculated to be $1.26 \times 10^6 \text{ m}^2 \text{ m}^{-3}$, and the model MSANS anisotropy is 1.23. The mean opening dimensions of the spheroidal pore systems together with their mean orientation distributions and the mean globular pore radius obtained by the model fit are given in Table 3. The fraction of specific surface area and void volume within the different void subsystems are compared in Table 4. Estimated errors of the model parameters are similar to the values given for the APS deposit.

Table 3. Modelled mean opening dimensions and orientation distributions for the WSP deposit.

	$\langle O.D. \rangle$ (μm)	$\langle 2R_G \rangle$ (μm)	g_L	g_M	g_H
$\beta = 1/10$	0.139	-	0.22	0.61	0.17
$\beta = 1/5$	0.279	-	0.27	0.54	0.19
Globular pores	-	2.720	-	-	-

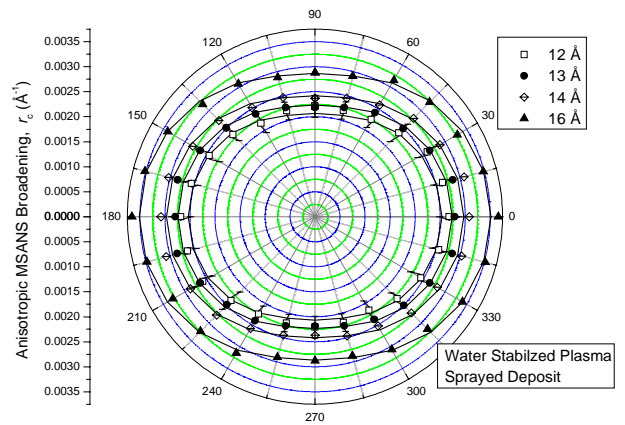


Fig. 5. MSANS anisotropy of the WSP cross-section sample with the spray direction perpendicular to the neutron beam.

Table 4. Specific surface areas and volume fractions of the three void subsystems for the WSP deposit, calculated from the MSANS model.

	Specific surface area [$10^6 \text{ m}^2 \text{ m}^{-3}$]	Volume fraction
$\beta = 1/10$	0.876 \cong 69 %	48 %
$\beta = 1/5$	0.338 \cong 27 %	35 %
Globular pores	0.046 \cong 4 %	17 %
Σ_{total}	1.260 \cong 100 %	0.119 \cong 100 %

Fig. 6 displays a SEM micrograph of a WSP deposit cross-section. Most of the spherical voids within the metallic matrix appear to be smaller than $\langle 2R_G \rangle = 2.72$ micrometer given by the model results (see table 4). This can be attributed to the influence of larger voids present between single splats.

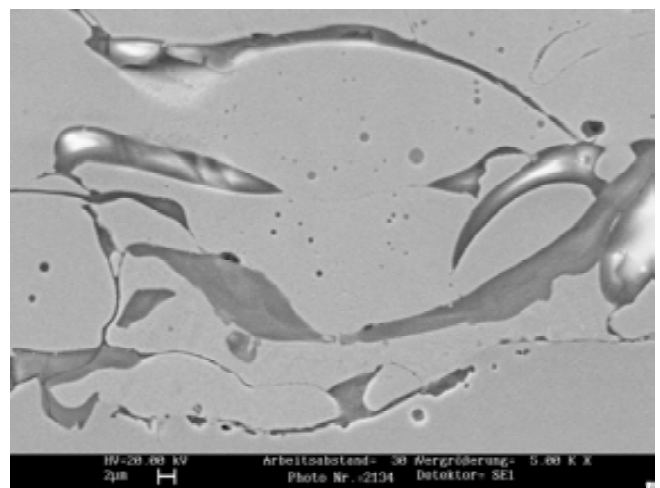


Fig. 6. SEM micrograph of a polished cross-section of the WSP NiCrAlY deposit. The spray direction is vertical.

4 Discussion and conclusion

The modelling of the MSANS broadening of thermally sprayed metallic NiCrAlY deposits allows three distinct void systems to be distinguished. In previous investigations on ceramic yttria-stabilized zirconia [2], the different void subsystems could be identified as: fine intralamellar cracks comprised of oblate spheroidal elements preferentially aligned perpendicular to the substrate, interlamellar pores also comprised of oblate spheroidal elements mainly aligned parallel to the substrate, and globular pores. Intralamellar cracks most likely originate from a release of residual stresses built up during the spray process. For the as-sprayed deposits, more than 0.20 of the total volume fraction was found to be in the intralamellar cracks [2].

In the present investigation on metallic NiCrAlY coatings, the fraction of total void volume in the globular pore system is 31 % for the APS deposit but only 17 % for the WSP deposit, corresponding to a void volume fraction of 0.025 for APS and 0.020 for WSP. The mean globular pore diameters, $\langle 2R_G \rangle$, are 1.89 micrometers and 2.72 micrometers, respectively. Their ratio of 1.4 suggests a larger globular pore diameter for the WSP deposit, which holds similarly for the mean opening dimensions of the two spheroidal element systems, since $\langle R \rangle_p / \langle R \rangle_c = 1.0$ and $\langle R \rangle_g / \langle R \rangle_c = 1.3$ were used for both deposits. Hence, the model suggests for the WSP deposit a on average 1.4 times larger size of the void elements compared to the APS sample, which is qualitatively in agreement with the SEM micrographs in Figs. 3 and 6. The main distinction between the deposits, predicted by the model, is found in the void volume fraction of the $\beta = 1/10$ void system: only 7 % for the APS deposit compared to 48 % for the WSP deposit. Further, for the WSP deposit, the orientation distribution is similar to that of the $\beta = 1/5$ void system.

For the APS deposit, an assignment of the $\beta = 1/10$ void system to intralamellar cracks and of the $\beta = 1/5$ void system to interlamellar pores is supported by the orientation distributions with preferential alignment perpendicular and parallel, respectively, to the substrate (g_L , g_M , g_H values in Table 1). The relatively low - compared to the ceramic yttria-stabilized zirconia - volume fraction of 7 % in the intralamellar crack system can be explained by a reduced generation of residual stresses and hence less cracking in the more ductile metal matrix.

However, for the WSP deposit, the model interpretation is different. For both the $\beta = 1/5$ and $\beta = 1/10$ void systems the short dimension of the spheroidal elements is mainly aligned within 0° - 30° and 30° - 60° to the spray direction as indicated in Table 3 (note, that for random distribution $g_L = 0.134$, $g_M = 0.366$ and $g_H = 0.5$, as mentioned in section 3). Hence, the $\beta = 1/10$ void system should be regarded as a further, interlamellar pore system. The two interlamellar model pore

systems thereby represent size distributions, that cannot be described by a single void model. A possible explanation, why a "crack" - type pore system is not explicitly found in the WSP deposit, might be the fact that for the water-stabilized plasma spray technique residual stresses are less significant than for the APS deposit.

Overall, the present results for the metallic NiCrAlY deposits suggest only a minor void component of fine "crack - like" pores with a preferred orientation perpendicular to the substrate. On the other hand, the interlamellar void systems account for most of the total porosity: 62 % of the APS deposit, and 83 % of the WSP deposit if the contributions from both interlamellar systems are added. These results strongly suggest that, for these deposits, macroscopic anisotropic material properties (e.g. elastic modulus, electrical [4] and thermal [11] conductivity) are dominated by the splat / interlamellar pore morphology.

5 Acknowledgment

We acknowledge the NIST Center for Neutron Research for the use of the SANS facility. Part of this work was funded by the EUREKA / KTI grant S1973 obtained by the THERMETCOAT project.

6 References

- [1] Ilavsky J., Long G.G., Allen A.J., Leblanc L., Prystay M., Moreau C., Proc. ITSC (1998), 1577.
- [2] Allen A.J., Ilavsky J., Long G.G., Wallace J.S., Berndt C.C., Herman H., Acta Mater. (2001), Issue 49, p. 1661.
- [3] Keller T., Wagner W., Ilavsky J., Margadant N., Siegmann S. et. al., Proc. 2nd Internat. Thermal Spray Conference (2001), p. 653.
- [4] Margadant N., Siegmann S., Patscheider J., Keller T., Wagner W. et al, Proc. 2nd Internat. Thermal Spray Conference (2001), p. 643.
- [5] Glinka C.J., Rowe J.M., LaRock J.G., J. Appl. Cryst., (1985), Issue 19, p. 427.
- [6] Porod G., in "Small Angle X-ray Scattering" edited by O. Glatter and O. Kratky, Academic Press, London, (1982), p. 17.
- [7] Schelten J., Schmatz W., J. Appl. Cryst. (1980), Issue 13, p. 385.
- [8] Berk N.F., Hardman-Ryhne K.A., J. Appl. Cryst. (1985), Issue 18, p. 467.
- [9] Allen A.J., Berk N.F., J. Appl. Cryst. (1994), Issue 27, p. 878.
- [10] Keller T., Wagner W., Allen A.J., Ilavsky J., Margadant N., Siegmann S., Kistorz G., submitted to Appl. Physics A. Material Science & Processing (supplement ICNS 2001).
- [11] Shafiro B., Kachanov M., J. Appl. Phys. (2000) Issue 87,12, p. 8561.